

# Deformation dynamics and spallation strength of aluminium under a single-pulse action of a femtosecond laser

S.I. Ashitkov, P.S. Komarov, A.V. Ovchinnikov, E.V. Struleva, M.B. Agranat

**Abstract.** An interferometric method is developed and realised using a frequency-modulated pulse for diagnosing a dynamics of fast deformations with a spatial and temporal resolution under the action of a single laser pulse. The dynamics of a free surface of a submicron-thick aluminium film is studied under an action of the ultrashort compression pulse with the amplitude of up to 14 GPa, excited by a femtosecond laser heating of the target surface layer. The spallation strength of aluminium was determined at a record high deformation rate of  $3 \times 10^9 \text{ s}^{-1}$ .

**Keywords:** femtosecond laser pulse, aluminium, strength.

## 1. Introduction

In recent years, increasing attention is paid to studying elastoplastic and strength properties of materials at limiting short durations of an applied load, realised with ultra-short laser pulses [1–7]. This refers to both fundamental problems of condensed-matter physics and applied aspects of development of laser material processing technologies. In particular, the strength of a material is known to substantially increase with the rate of its extension [8]. The limiting value of strength or so-called ideal strength corresponds to the condensed state spinodal of the matter. A calculated value of the ideal tensile strength for aluminium is 11.7 GPa [9]. One may approach an ideal strength by increasing the deformation rate of the material  $\dot{\epsilon}$ , which is attained either by shortening the duration of an impact load or by increasing its amplitude. Presently, highest deformation rates  $\dot{\epsilon} \sim 10^8\text{--}10^9 \text{ s}^{-1}$  were obtained in laser experiments with pico- and femtosecond pulses [1, 3, 7]. In those experiments, the measured tensile strength of aluminium  $\sigma_{\text{spall}}$  was above 50% relative to the ideal strength.

In laser shock-wave experiments the value of  $\sigma_{\text{spall}}$  is usually determined by either measuring the spallation cave depth [7] or recording the profile of a free surface velocity  $u_{\text{fs}}(t)$  for the sample under investigation. In the latter case, various fast interferometric methods are employed. The accuracy of a laser Doppler velocity meter ORVIS with an electro-optical

signal recording used in [1] was insufficient for studying processes with deformation velocities of above  $10^8 \text{ s}^{-1}$ . The method of interferometer microscopy used in [3] in the pump-probe measuring scheme with a varied delay between the heating and probe pulses has a drawback of multiple action on a sample under test. In the case of shock-wave experiments this imposes sufficiently strict technical conditions on the stability of laser pulse parameters and, more important, on uniformity of optical properties and thickness of the samples.

Recent trends are toward new high-speed diagnostic methods which provide recording of the process dynamics under the action of a single laser pulse with a time resolution of  $\sim 10^{-12} \text{ s}$  by using a frequency-modulated (chirped) pulse as the probe signal. These methods were earlier used for studying shock-wave propagation in polymethylmethacrylate [10] and elastoplastic properties of metals [5, 6]. The approach is based on the fact that different spectral components of a chirped pulse arrive at a target at different instants.

In the present work, the interferometric method is realised with employment of a diagnostic chirped pulse for studying a dynamics of fast deformations arising in a material under a single-exposed laser action. Employment of the method provided obtaining new data on the aluminium spallation strength at currently record high deformation rates. In addition, single-exposure measurements are more reliable and can be applied to studying the statistics of spallation phenomena in samples possessing not high uniformity.

## 2. Experiment

An optical scheme of the experiment is shown in Fig. 1. The radiation source was a Ti:sapphire laser system. The pulses of duration 30 fs with a centre wavelength of 790 nm and spectral width of 40 nm emitted by a driving generator were directed to a stretcher with a diffraction grating  $1200 \text{ mm}^{-1}$  for time-domain expansion. After the stretcher the chirped pulse was amplified in a regenerative amplifier to the energy of 2 mJ. Then the laser beam was split into two parts. The more powerful pump pulse passed to a time-domain compressor for shortening to the duration of 40 fs. The other frequency-modulated 300-ps diagnostic pulse passed through an optical delay to a Michelson interferometer.

An aluminium film of thickness 760 nm formed by a magnetron deposition on a 150- $\mu\text{m}$ -thick glass substrate was used as a sample. According to results of modelling [11], under the action of femtosecond pulses with the intensity of  $\sim 10^{13} \text{ W cm}^{-2}$  a shock-wave in aluminium is formed already at a path length of 500–600 nm.

The pump pulse was focused by a lens with a focal length of 30 cm through a substrate onto a surface of the metal film

S.I. Ashitkov, P.S. Komarov, A.V. Ovchinnikov, E.V. Struleva, M.B. Agranat Joint Institute for High Temperatures, Russian Academy of Sciences, Izhorskaya ul. 13, Bld. 2, 125412 Moscow, Russia; e-mail: ashitkov11@yandex.ru, komarov-p@yandex.ru, ovtch2006@rambler.ru, struleva.evgenia@yandex.ru, agranat2004@mail.ru

Received 24 December 2012

Kvantovaya Elektronika 43 (3) 242–245 (2013)

Translated by N.A. Raspopov

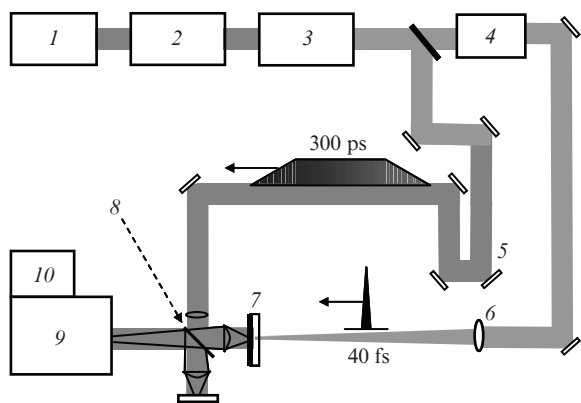


**Figure 1.** Optical scheme of measurements: (1) seed oscillator; (2) stretcher; (3) regenerative amplifier; (4) compressor; (5) optical delay; (6) lens; (7) sample; (8) Michelson interferometer; (9) spectrometer; (10) CCD-camera.

in a spot 70  $\mu\text{m}$  in diameter by the level  $1/e$  with the Gaussian intensity distribution. The pulse energy might be smoothly varied by a polarisation attenuator and was measured by a calibrated photodetector. Absorption of the pump radiation in the metal surface layer was accompanied with generation of the shock compression pulses propagating toward the backside free surface of the sample resulting in a deformation of the latter. After each laser pulse the sample under test was moved to a new position by a three-dimensional micromanipulator.

A diagnostic unit of the scheme comprised a Michelson interferometer [3, 12]. A micro-objective with a numerical aperture of  $\text{NA} = 0.2$  was used to transfer the backside sample image with an  $8\times$  magnification to the entry slit of a diffraction spectrometer Acton 2300i. The spectrometer was adjusted in such a way that the interference fringes were perpendicular to the entry slit. The image at the output of the spectrometer was recorded by a 12-bit CCD-camera.

If the diagnostic pulse is frequency-modulated then the wavelength axis in the recorded spectrum may be juxtaposed to the time scale  $t$ , whereas the other axis (along the slit of the spectrometer) would correspond to one of the spatial coordinates in the target plane. In the scheme under consideration, the spatial resolution in the target plane  $xy$  was determined by the objective numerical aperture and was equal to  $\sim 2 \mu\text{m}$ .

The shift of target surface due to a passing compression pulse results in a change of the phase relation between the object and reference beams, which shifts the interference fringes. Spatiotemporal interference fringes  $I(y, t)$  are processed by using a two-dimensional Fourier transform thoroughly described in [12], which gives a 2D image of the phase variation  $\Delta\varphi(y, t)$  of the diagnostic pulse in the interaction region in the space–time coordinates. The value of the surface shift  $\Delta z$  is related to the phase variation by the relationship  $\Delta z(y, t) = \lambda(t)\Delta\varphi(y, t)/(4\pi)$ . In this case, the inaccuracy of phase measurements  $\delta\varphi \approx \pi/100$  realised in the considered scheme corresponds to that of the surface shift and equals to 2–3 nm.

The time scanning was calibrated by varying the length of the optical delay line between the heating and probing pulses. In this case, the initial instant of a phase change  $\Delta\varphi$  was detected that was related to arrival of the compression pulse to the backside surface of the target. The measurements performed show (Fig. 2) that the wavelength dependence on time

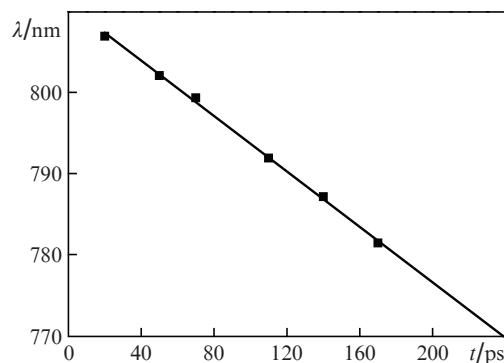


**Figure 2.** Wavelength  $\lambda$  vs. time  $t$  in the diagnostic frequency-modulated pulse.

in the frequency-modulated pulse is of linear character within the measurement error. With the 600 lines  $\text{mm}^{-1}$  grating employed in the spectrometer, the concurrently recorded time interval was 235 ps. The time resolution was determined in this case by the spectrometer resolution and was equal to 2 ps.

### 3. Results and discussion

A spatiotemporal distribution of the phase variation  $\Delta\varphi(y, t)$  for the diagnostic pulse is shown in Fig. 3. It describes the deformation dynamics of the backside free surface of the aluminium film as the compression pulse arrives that is created due to heating of the target front surface by the femtosecond laser pulse. The  $y$  axis coincides with the cross section passing through a centre of an interaction zone.

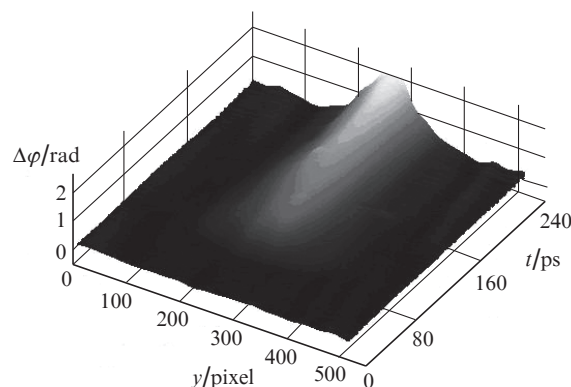


**Figure 3.** Spatiotemporal distribution of phase variation  $\Delta\varphi(y, t)$  of the diagnostic pulse after the shock wave arrival to a free surface of the 760-nm-thick aluminium film after the action of a single heating pulse with a duration of 40 fs and energy density of  $F_0 = 2 \text{ J cm}^{-2}$ .

Shift profiles  $z$  and velocities  $u_{fs}$  of the free surface of aluminium sample are shown in Fig. 4 versus time. The profiles  $z(t)$  are obtained in a single laser shot by processing a spatiotemporal phase distribution  $\Delta\varphi(y, t)$  (Fig. 3) for two different values of the spatial coordinate  $y$  corresponding to different intensities of the laser pulse. Curve (1) in Fig. 4 corresponds to a central part of the interaction zone where the energy density  $F_0$  of an incident radiation was maximal and equal to  $2 \text{ J cm}^{-2}$ ; curve (2) corresponds to a peripheral part of the focal spot with  $F = 1.4 \text{ J cm}^{-2}$ . The rate profiles in Fig. 4 are obtained by differentiating smoothed-out dependences  $z(t)$ .

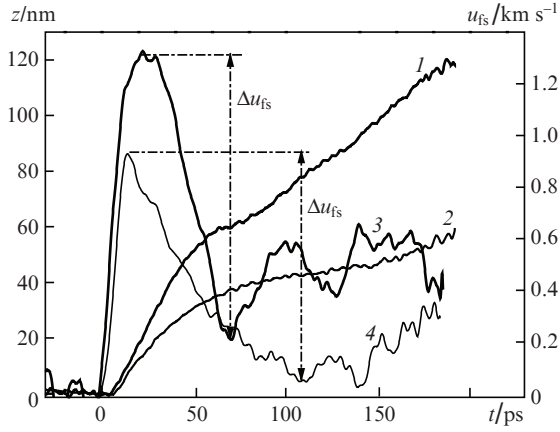


**Figure 4.** Shift  $z$  (1, 2) and velocity  $u_{fs}$  (3, 4) of a free backside surface of the 760-nm-thick aluminium sample vs. time after the action of a laser pulse with a duration of 40 fs and energy density of  $F_0 = 2 \text{ J cm}^{-2}$  (1, 3) and  $F = 1.4 \text{ J cm}^{-2}$  (2, 4).

Figure 5 shows the measurement results of the deformation dynamics of the backside free surface for a similar aluminium sample [3] obtained by femtosecond interference spectroscopy. In those experiments, the dependence  $z(t)$  was measured pointwise under multiple laser action on target at a varied time delay between the heating and probing pulses.

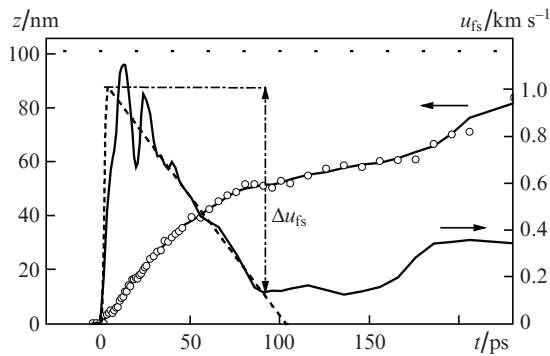


**Figure 5.** Shift  $z$  of a free surface of the 760-nm-thick sample vs. time after the action of the laser pulse with a duration of 150 fs and energy density of  $F_0 = 1.3 \text{ J cm}^{-2}$  (points refer to an experiment). The velocity profile  $u_{fs}(t)$  was obtained by differentiating a smoothed experimental dependence  $z(t)$ , dashed line refers to a initial part of the profile  $u_{fs}(t)$  obtained from approximation of experimental data by a square law curve.

A comparison of results of the two measurement methods at close parameters of the laser pulses [curves (2, 4) in Fig. 4 and the corresponding dependences  $z(t)$  and  $u_{fs}(t)$  in Fig. 5] demonstrate their good coincidence.

The value of pressure  $p$  behind the shock-wave wavefront is determined by the expression

$$p = \rho_0 U_s u_p, \quad (1)$$

Here  $\rho_0$  is the initial density of material;  $U_s$  is the speed of shock wave propagation; and  $u_p = u_{fs}^{\max}/2$  is the particle velocity behind the wavefront of the latter, which is half the peak value of the free surface speed. Results of recent investigations [3, 4] revealed that in the considered conditions the uni-

directional compression in aluminium is of elastic character. In this case, the coefficients in the linear expression for the elastic compression

$$U_s = c_0 + b u_p \quad (2)$$

take the values  $c_0 = 6.4 \text{ km s}^{-1}$ ,  $b = 1.8$ .

As one can see from profiles  $u_{fs}(t)$  in Fig. 4, the ultrashort shock compression pulse at the exit from the sample has a triangular shape with the half-height characteristic duration of  $\tau_s \approx 50 \text{ ps}$  and the leading-edge time on the order of several picoseconds. In this case, the maximal amplitude of the compression pulse is, according to (1) and (2) as high as 13.7 GPa.

A compression pulse reflected from the free sample surface gives rise to a tensile stress increasing as the reflected wave propagates from the surface inside the sample. In the case where the tensile stress becomes greater than the material strength  $\sigma_{\text{spall}}$ , a spallation fracture arises [8, 13]. Relaxation of stresses in the breakdown leads to origin of the secondary compression wave, which reaching the free surface causes a secondary increase in the surface speed (spallation pulse). The value of the tensile stress just before the breakdown can be determined using the method of characteristics by the fall of speed  $\Delta u_{fs}$  from its maximal value to the value immediately ahead of the spallation pulse (Fig. 4). The acoustic approximation [1] often used in literature for determining the spallation strength  $\sigma_{\text{spall}} = \rho_0 c \Delta u_{fs} / 2$  makes no allowance for a non-linearity of material compressibility and, hence, overestimates  $\sigma_{\text{spall}}$ . The nonlinearity can be taken into account by extrapolating shock adiabat (2) to negative pressure values. This results in the following expression for determining the spallation strength [14]:

$$\sigma_{\text{spall}} = \frac{1}{2} \rho_0 \left( c_0 - b \frac{\Delta u_{fs}}{2} \right) \Delta u_{fs}. \quad (3)$$

The rate of deformation  $\dot{\epsilon}$  is characterised by the speed of material expansion in the discharge part of the incident compression pulse and is determined by the expression [1, 8]:

$$\dot{\epsilon} = \frac{\dot{V}}{V_0} = \frac{\dot{u}_{fs}}{2c_0}, \quad (4)$$

the thickness of the spallation layer can be obtained from the relationship

$$L_{\text{spall}} = \frac{c_0 (t_{\min} - t_{\max})}{2}, \quad (5)$$

where  $t_{\max}$  and  $t_{\min}$  are the instants at which the parameter  $u_{fs}$  takes, correspondingly, its maximal and minimal values prior to arrival of the spallation pulse.

In view of (1), (4) from the measured velocity profiles  $u_{fs}(t)$  (Fig. 4) it follows that in increasing the amplitude of shock compression from 9.1 to 13.7 GPa the spallation strength  $\sigma_{\text{spall}}$  of the aluminium sample under investigation raised from 6.7 to 8.4 GPa. The rates of expansion  $\dot{\epsilon}$  at these values of  $p$  were, correspondingly,  $1.5 \times 10^9$  and  $3 \times 10^9 \text{ s}^{-1}$ , and the thickness of spall according to (5) reduced from 300 to 150 nm.

In the present work, data on aluminium spallation strength are obtained at presently record high deformation rates of up to  $3 \times 10^9 \text{ s}^{-1}$ . In contrast to earlier experiments [3], higher values of  $\dot{\epsilon}$  are related with an increased amplitude of shock compression pulses due to a higher energy density of the heating pulses. Earlier [3], in the measurements with fem-

to-second interferometer spectroscopy the limitation on the parameter  $F_0 \leq 1.3 \text{ J cm}^{-2}$  was related with necessity of performing the measurements a fortiori below the optical breakdown threshold of target glass substrates in order to enhance the reproducibility of compression pulse parameters from shot to shot.

#### 4. Conclusions

Thus, we have developed and realised the interferometric method for studying fast deformations caused by the action of high-power femtosecond laser pulses. The method provides recording of the dynamics of this process under the action of single-short laser radiation in the time interval 0–240 ps with the time resolution of 2 ps, spatial resolution of 2  $\mu\text{m}$  and accuracy of surface shift measurements of 2–3 nm. The dynamics of motion of the backside free surface of an aluminium film was investigated under the action of the shock compression pulse with the duration of  $10^{-10}$  s and amplitude of up to 13.7 GPa. The spallation strength of aluminium was determined at record high strain rate of  $3 \times 10^9 \text{ s}^{-1}$ . The investigation results for the aluminium deformation dynamics obtained in the present work well agree with data from [3] obtained by the method of femtosecond interferometer microscopy.

**Acknowledgements.** The work was supported by programmes ‘Extreme Light Fields and Their Applications’ and ‘Substance under High Energy Densities’ of the Presidium of the Russian Academy of Sciences and by the Russian Foundation for Basic Research (Grant No. 11-08-12107-ofi-m-2011).

#### References

1. Eliezer S., Moshe E., Eliezer D. *Laser Part. Beam*, **20**, 87 (2002).
2. Gahagan K.T., Moore D.S., Funk D.J., Rabie R.L., Buelow S.J., Nicholson J.W. *Phys. Rev. Lett.*, **85**, 3205 (2000).
3. Ashitkov S.I., Agranat M.B., Kannel G.I., Komarov P.S., Fortov V.E. *Pis'ma Zh. Eksp. Teor. Fiz.*, **92**, 568 (2010) [*JETP Lett.*, **92**, 516 (2010)].
4. Zhakhovskii V.V., Inogamov N.A. *Pis'ma Zh. Eksp. Teor. Fiz.*, **92**, 574 (2010) [*JETP Lett.*, **92**, 521 (2010)].
5. Whitley V.H., McGrane S.D., Eakins D.E., Bolme C.A., Moore D.S., Bingert J.F. *J. Appl. Phys.*, **109**, 013505 (2011).
6. Crowhurst J.C., Armstrong M.R., Knight K.B., Zaug J.M., Behymer E.M. *Phys. Rev. Lett.*, **107**, 144302 (2011).
7. Abrosimov S.A., Bazhulin A.P., Voronov V.V., Krasnyuk I.K., Pashinin P.P., Semenov A.Yu., Stuchebyukhov I.A., Khishchenko K.V. *Dokl. Ross. Akad. Nauk*, **442**, 752 (2012).
8. Kannel G.I., Fortov V.E., Razorenov S.V. *Usp. Fiz. Nauk*, **177**, 809 (2007) [*Phys. Usp.*, **50**, 771 (2007)].
9. Sin'ko G.V., Smirnov N.A. *Pis'ma Zh. Eksp. Teor. Fiz.*, **75**, 217 (2002).
10. Babin A.A., Kiselev A.M., Kulagin D.I., Pravdenko K.I., Stepanov A.N. *Pis'ma Zh. Eksp. Teor. Fiz.*, **80**, 344 (2004).
11. Anisimov S.I., Inogamov N.A., Petrov Y.V., Khokhlov V.A., Zhakhovskii V.V., Nishihara K., Agranat M.B., Ashitkov S.I., Komarov P.S. *Appl. Phys. A*, **92**, 797 (2008).
12. Temnov V.V., Sokolovski-Tinten K., Zhou P., Von der Linde D. *J. Opt. Soc. Am. B*, **23**, 1954 (2006).
13. Zeldovich Ya.B., Raizer Yu.P. *Physics of Shock Waves and High-Temperature Hydrodynamic Phenomena* (New York: Acad. Press, 1966; Moscow: Nauka, 1966).
14. Kannel G.I. *Zh. Prikl. Mekh. Tekhn. Fiz.*, **42**, 194 (2001) [*J. Appl. Mech. Techn. Phys.*, **42**, 358 (2001)].